Biosensors and Bioelectronics 35 (2012) 277–283

Contents lists available at SciVerse ScienceDirect

Biosensors and Bioelectronics

journal homepage: www.elsevier.com/locate/bios

A novel immunosensor based on an alternate strategy of electrodeposition and self-assembly

Yiming Zhang[1], Huan Chen, Xia Gao, Zhichun Chen, Xianfu Lin*

Department of Chemistry, Zhejiang University, Hangzhou 310027, PR China

ARTICLE INFO

Article history:
Received 31 December 2011
Received in revised form 23 February 2012
Accepted 28 February 2012
Available online 30 March 2012

Keywords:
Multiwalled-carbon nanotubes
Gold nanoparticles
Electrodeposition
Self-assembly
Prussian blue
Immunosensor

ABSTRACT

A novel amperometric immunosensor for the determination of carcinoembryonic antigens (CEA) was developed. Firstly, ordered multilayer films of Prussian blue (PB) and multiwalled-carbon nanotube/polyethylenimine/Au (MWNT–PEI–Au) nanocomposite were fabricated onto the surface of a glassy carbon electrode via alternate electrodeposition and self-assembly. Then a layer of chitosan mixed with gold nanoparticles was cast onto the surface of the electrode. Subsequently, the electrode was coated with antibody (Ab_1) and blocked with BSA. The morphology of the MWNT–PEI–Au nanocomposite was characterized by transmission electron microscopy (TEM). The fabrication process of the ordered multilayer structure and immunosensor were characterized by scanning electron microscopy (SEM) and electrochemical measurements, respectively. The proposed fabrication strategy effectively ensured the stability of the Prussian blue as electron mediator. Under optimal conditions, the fabricated immunosensor exhibited a good response to CEA, with a detection range from 0.5 to 160 ng/mL and a detection limit of 0.08 ng/mL at 3δ. The current fabricated immunosensor exhibited good sensitivity, selectivity, and long-term stability. Furthermore, current study demonstrated the promising application of the alternate strategy based on electrodeposition and self-assembly for the construction of biosensor.

1. Introduction

In past decades, the determination of tumor markers was an important topic in the field of clinical analysis. Although several methods can be chosen for the determination of tumor markers, including conventional enzyme immunoassay (Clerico et al., 2000; Worwood, 2002; Hage, 1999), radioimmunoassay (Cioffi et al., 2001), and fluoroimmunoassay (Matsumoto et al., 1999), immunosensors have attracted increasing interest because of their easy operation, low cost, and ability to be implemented at the point-of-care (PoC) (Tlili et al., 2010). Among these immunosensors, electrochemical immunosensors are the most promising because of their high sensitivity, ease of use and portability (Munge et al., 2009; Ou et al., 2007).

Many reported amperometric immunosensors utilized the electrolyte containing reversible redox species, such as ferricyanide (Gao et al., 2011), thionine (Wu et al., 2006), because most antigen or antibody proteins do not have electrochemical activity. However, the redox compounds in the supporting electrolyte may affect the bioactivity of antibodies or antigens (Shi and Ma, 2011). In order to improve the analytical performance of immunosensor and simplify immunoassay operation, the label-free immunosensor based on the immobilization of electron mediators onto the interface of electrode has attracted much attention. Here, many types of mediators have been applied to the construction of immunosensors in the literature, such as Prussian blue (PB), ferrocene and its derivatives (Qiu et al., 2009), phenazine dye (Chai et al., 2008; Zhuo et al., 2005), and 3,3′,5,5′-tetramethylbenzidine (TMB) (Wu et al., 2009). Among those mediators, the PB has been extensively used in the construction of biosensors because of its low cost, versatility of preparation and good redox activity (Karyakin et al., 1995; Haghighi et al., 2004; Jiang et al., 2010; Song et al., 2010; Ou et al., 2008).

The effective and stable immobilization of electron mediators onto the conducting interface of label-free immunosensors is a key point for the fabrication of immunosensors. Different immobilization methods of mediators on the surface of biosensors had been utilized, including cast method, layer-by-layer assembly (LbL) and electrodeposition. Although one-step electrodeposition can provide a direct, simple and quick way to construct a PB layer on the surface of electrodes, modified electrodes usually show unstable electrochemical performance due to the unsatisfied stability of the PB layer (Karyakin et al., 1995; Haghighi et al., 2004). To improve

* Corresponding author. Tel.: +86 571 87953001; fax: +86 571 87952618.
E-mail address: llc123@zju.edu.cn (X. Lin).
[1] Address: Hangzhou Center for Disease Control and Prevention, Hangzhou 310021, PR China.

0956-5663/$ – see front matter © 2012 Elsevier B.V. All rights reserved.
doi:10.1016/j.bios.2012.02.063

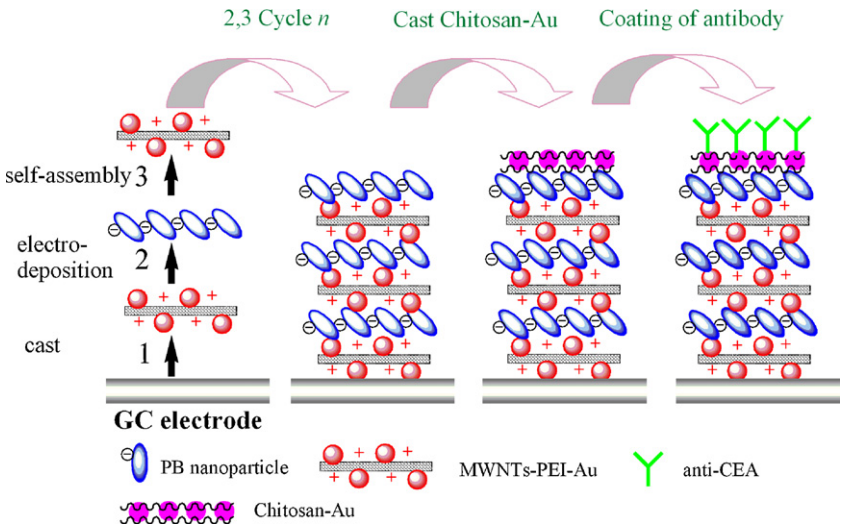

Scheme 1. The construction process of the immunosensors.

the stability of PB layer, MWNT and gold nanoparticles were introduced into the electrodeposition process of PB layer, but slow signal attenuation was still observed (Li et al., 2007; Sharma et al., 2011).

As an important fabrication method, LbL self-assembly technique could offer an effective approach to the fabrication of ordered multilayer films with controlled composition and thickness. Ordered structure of multilayer film can provide a favorable microenvironment to maintain the stability of film matrix (Liu and Lin, 2006). Yuan group reported several works about the multilayer PB nanoparticle modified immunosensor based on LbL technique. For example, Ou et al. (2008) utilized the Pt–PB hybrid nanoparticles and MWNT–chitosan to construct an immunosensor via LbL assembly. Therefore, the combination of electrodeposition and layer-by-layer self-assembly as a strategy for stable immobilization of electron mediators on the electrode surface may provide quick fabrication of the stable interface of immunosensors with ordered multilayer structure, and should be an interesting study topic.

This work attempted to construct an immunosensor based on an alternate strategy combining electrodeposition and the self-assembly technique. The PB nanoparticles and synthesized multiwalled-carbon nanotube/polyethylenimine/Au (MWNT–PEI–Au) nanocomposite were incorporated into the fabrication process. Through the alternate strategy of electrodeposition of PB nanoparticles and the self-assembly of a MWNT–PEI–Au nanocomposite highly stable and ordered $(MWNT–PEI–Au/PB)_n$ composite films were obtained, which also acted as a good matrix for electron transfer. Finally, a layer of chitosan–Au film covered onto the surface of the electrode to form the coating layer for immobilization of the antibody. Here, carcinoembryonic antigen (CEA) was used as a model substrate. The prepared immunosensor showed high sensitivity, low detection limit and long-term stability.

2. Experimental

2.1. Materials and reagents

Multiwalled-carbon nanotubes (10–20 nm in diameter, 95%) were purchased from Shenzhen Nanotech Port Co., Ltd. (Shenzhen, China). The purification and carboxylation of the MWNT were performed according to our previous report (Liu et al., 2008). Polyethylenimine (PEI, branched, Mw 10,000), potassium ferricyanide ($K_3Fe(CN)_6$), potassium ferrocyanide ($K_4Fe(CN)_6{\cdot}4H_2O$), iron(O) chloride hexahydrate ($FeCl_3{\cdot}6H_2O$), hydrogen tetrachloroaurate ($HAuCl_4{\cdot}4H_2O$), and potassium chloride (KCl) were purchased from the Chemical Reagent Company of Shanghai (Shanghai, China). All of the reagents were of analytical grade, and double distilled water was used throughout the experiments.

Chitosan (Mw = 1,000,000, deacetylation degree 92%) and bovine serum albumin (BSA) were purchased from the Chemical Reagent Company of Shanghai (Shanghai, China). Anti-carcinoembryonic antigen (anti-CEA, Ab_1) and carcinoembryonic antigen (CEA) were purchased from Beijing Keyuezhongkai Biotechnical Company (Beijing, China) and kept at −20 °C.

Glassy carbon electrodes with diameters of 4 mm were purchased from CHI Instruments (Shanghai, China). Indium–tin oxide (ITO) conducting glass was obtained from Laibao Hi-Tech Co., Ltd. (Shenzhen, China).

2.2. Preparation of the MWNT–PEI–Au nanocomposite

The MWNT–PEI–Au nanocomposite was prepared according to the literature, with necessary modifications (Hu et al., 2006; Zhang et al., 2012). This suspension was highly dispersible and was stable for two months at room temperature. The nanocomposite of MWNT–PEI was fabricated in a similar fashion without the addition of the $HAuCl_4$ aqueous solution.

2.3. Formation of $(MWNT–PEI–Au/PB)_n$ multilayer composite films

The pre-treatment of the glassy carbon (GC) electrode was performed according to the literature (Cui et al., 2008). First, 5 μL of MWNT–PEI–Au nanocomposite was cast onto pre-treated substrate and dried at room temperature. Then the substrate was dipped into a 2.5 mM $K_3Fe(CN)_6$ and 2.5 mM $FeCl_3$ solution containing 0.1 M KCl and 0.1 M HCl, and the electrodeposition was performed by cyclic voltammetry between 0.4 and −0.1 V at a scan rate of 50 mV/s for five cycles. Afterwards, the substrate was rinsed with double-distilled water and dried under nitrogen. Next, 10 μL of the MWNT–PEI–Au nanocomposite was cast onto the surface of the substrate for self-assembly for 30 min in a wet chamber at room temperature. These processes were repeated to obtain the $(MWNT–PEI–Au/PB)_n$ composite film.

2.4. Construction of the immunosensor

The synthesis of gold nanoparticles was performed according to the literature (Grabar et al., 1995), and the diameter of the final synthesized nanoparticle was approximately 16 nm. Through centrifugation, the original synthesized gold nanoparticle suspension was concentrated 10-fold. Then 100 μL of the concentrated gold nanoparticle suspension was added into a 1% chitosan solution, and the dispersion was sonicated for 10 min to generate a homogeneous mixture of chitosan–Au. Next, 5 μL of chitosan–Au suspension was cast onto the surface of a $(MWNT–PEI–Au/PB)_n$-modified electrode and dried at room temperature. Subsequently, 20 μL of anti-CEA (500 μg/mL, in 0.01 M PBS buffer, pH 7.2) was dropped onto the surface of the modified electrode at 4 °C for approximately 12 h. Finally, the modified electrode was incubated in a 0.5% (w/w) BSA solution for 2 h at room temperature to block the remaining active sites and avoid non-specific adsorption. The resulting immunosensor was stored at 4 °C when not in use. The entire fabrication procedure is shown in Scheme 1.

2.5. Apparatus and measurements

The morphologies of the assembled multilayer films were observed using a Sirion-100 field-emitting scanning electron microscope (SEM, FEI, USA). The surface morphology of the MWNT–PEI–Au nanocomposite was visualized using transmitting electron microscopy (TEM, JOEL, Japan).

Electrochemical measurements were performed with a CHI 650c electrochemical workstation (Shanghai CH Instrument Company, China). A conventional three-electrode system was used with a platinum disk electrode as the auxiliary electrode, a saturated calomel electrode (SCE) as the reference electrode and a modified GC electrode as the working electrode. Cyclic voltammograms (CV) were performed in 0.025 M PBS containing 0.1 M KCl (pH 6.0) from 0.4 to −0.1 V at a scan rate of 50 mV/s. For CEA detection, the changes in reduction peak current (ΔI) before and after antigen–antibody reaction were calculated in the equation $\Delta I = I_0 - I$, where I represents the peak current after immunoreactions, and I_0 represents the peak current before immunoreactions.

3. Results and discussion

3.1. Formation of the $(MWNT–PEI–Au/PB)_n$ nanocomposite multilayer films

Fig. 1 shows the CVs of electrodes modified with different numbers of (MWNT–PEI–Au/PB) bilayers in 0.025 M PBS (containing 0.1 M KCl, pH 6.0). All of the electrodes gave well-defined redox peaks, and the increased peak current was proportional to the numbers of bilayers, which suggests that the electrochemical signal could be effectively enhanced through the alternate cycles of electrodeposition and self-assembly. For the first layer of MWNT–PEI–Au prepared by the casting method, thus, the inset of Fig. 1 shows the linear correlations between the reduction current and the number of bilayers from two to seven. These results confirmed that the alternate strategy of electrodeposition and self-assembly was feasible and led to the formation of ordered and functionalized composite films.

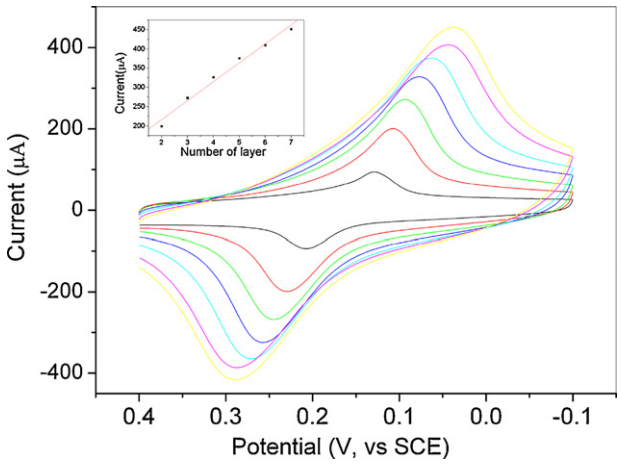

Fig. 1. CVs response after successive alternate electrodeposition and self-assembly; the supporting electrolyte was 0.025 M PBS containing 0.1 M KCl, pH 6.0. Inset: Anodic peak current vs. number of fabricated nanocomposite bilayers.

The TEM image of the MWNT–PEI–Au nanocomposite is shown in the inset of Fig. 2a. It was clear that gold nanoparticles were anchored around the sidewalls of the MWNT, which agreed with the results published in the literature (Hu et al., 2006). Fig. 2a also shows the surface morphologies of the ITO slides modified by the MWNT–PEI–Au nanocomposite. The MWNT–PEI–Au nanocomposite was firmly and uniformly adsorbed through strong electrostatic interactions, and the Au nanoparticles were scattered on the surface of the MWNT.

After five cycles of electrodeposition, the surface of the MWNT–PEI–Au nanocomposite became rougher, and the diameter of the MWNT became larger, which implies that the PB nanoparticles were successfully deposited on the surface of the MWNT–PEI–Au nanocomposite (Fig. 2b). In the inset of Fig. 2b, the magnified zone highlights PB nanoparticles covering the MWNT nanocomposites. These results may be attributed to the positive charge of the MWNT–PEI–Au nanocomposite and the negative charge of the PB nanoparticles (Fiorito et al., 2005). Here, the PEI acted as a bridge role to connect the MWNT and PB nanoparticles

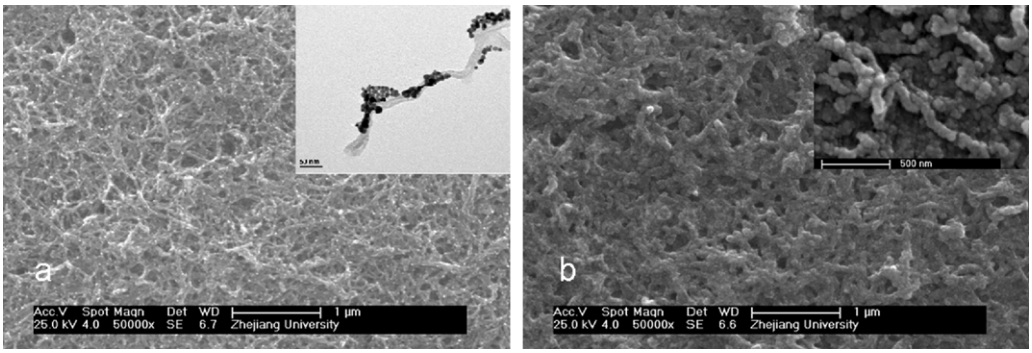

Fig. 2. The morphologies of MWNT–PEI–Au (a), inset of a: the TEM details for the morphology of MWNT–PEI–Au and MWNT–PEI–Au/PB (b), inset of b: a local magnified zone of MWNT–PEI–Au/PB.

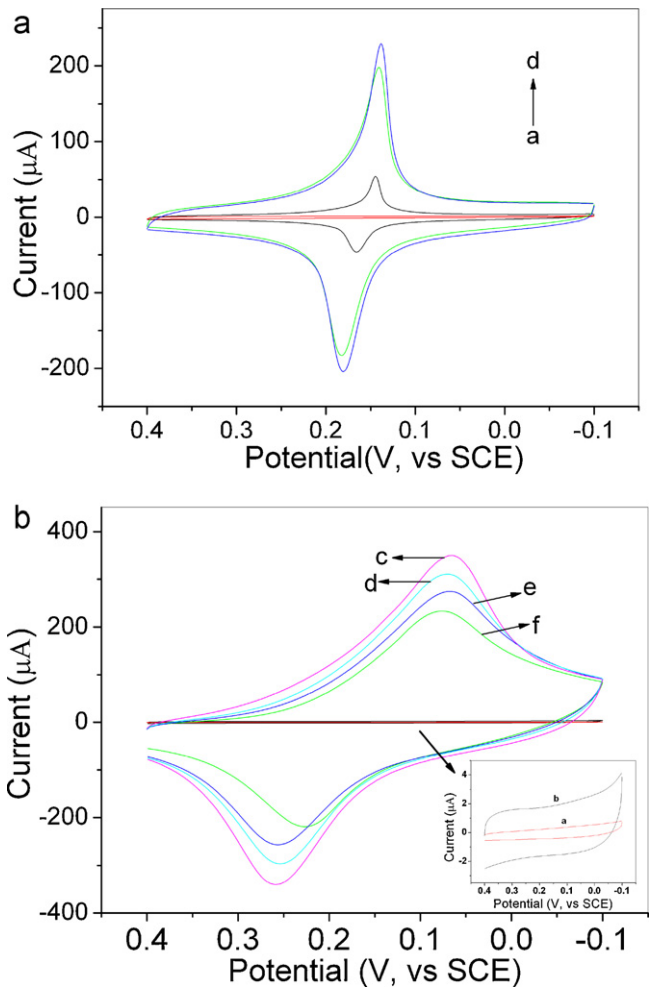

Fig. 3. (A) The CVs of different modified electrodes in a 0.1 M KCl solution containing 0.1 M HCl (scan rate: 50 mV/s vs. SCE). From inside to outside: $(PEI/PB)_3$, bulk PB, $(MWNT–PEI/PB)_3$ and $(MWNT–PEI–Au/PB)_3$. (B) The CV characterizations of different modified electrodes: bare GC (a); GC/MWNT–PEI–Au (b); $(MWNT–PEI–Au/PB)_5$ (c); $(MWNT–PEI–Au/PB)_5$/(chitosan–Au) (d); $(MWNT–PEI–Au/PB)_5$/(chitosan–Au)/Ab_1 (e); $(MWNT–PEI–Au/PB)_5$/(chitosan–Au)/Ab_1/BSA (f). The supporting electrolyte solution was 0.025 M PBS containing 0.1 M KCl, pH 6.0.

because of the PB can stably bind to the polymer chain (Hornok and Dékány, 2007). In addition, the bulk PB layer onto the smooth ITO fabricated under the same conditions can be seen clearly, indicating the current PB layer was composed of uniform nanoparticles (see Supplementary Fig. S1).

3.2. Electrochemical characterization of the composite films

Fig. 3A shows the CVs of different electrodes modified with $(MWNT–PEI–Au/PB)_3$, $(MWNT–PEI/PB)_3$, $(PEI/PB)_3$ and bulk PB. In contrast to the electrode modified by bulk PB, the electrode modified with $(PEI/PB)_3$ displayed only weak redox peaks. As a non-conducting polymer, PEI may impede the electron transfer on the surface of the electrode. Thus, the PB nanoparticles could not effectively grow on the surface of the PEI-modified electrode without carbon nanotubes. These results confirm the function of MWNT as a conductive matrix material. The behavior of the $(MWNT–PEI–Au/PB)_3$-modified electrode was similar to that of the electrode modified with the $(MWNT–PEI/PB)_3$, but with a higher current response. This result may be attributed to the function of Au nanoparticle, which acted as electron antenna, further improved conductivity of modified interface on the electrode.

On the other hand, the signal attenuation of immunosensors in the supporting electrolyte is unfit for accurate determination based on the blocking effect. The different manner of deposition employed for PB seemed to affect the stability of the fabricated sensor (Ricci and Palleschi, 2005). Compared with the sensors modified with $(MWNT-PEI/PB)_3$ or bulk PB, the $(MWNT–PEI–Au/PB)_3$ film showed the best stability. Through successive CVs in the supporting electrolyte within 2 h, the $(MWNT–PEI–Au/PB)_3$ modified electrode did not show any observable decrease of peak current. The probable causes may be attributed to the following factors. First, the polyelectrolyte and MWNT effectively enhanced the electrochemical stability of PB (Li et al., 2007; Lukachova et al., 2002). In addition, it was reported that the stability of the PB layer was effectively improved through the deposition of PB onto the gold nanocrystals (Song et al., 2010). In this study, Au nanoparticles on the surface of MWNT might further enhance this protective action of MWNT and polyelectrolytes for PB nanoparticles. Furthermore, the constructed sandwich-like multilayer structure might also provide a favorable microenvironment to stabilize PB layer. Therefore, the stability of $(MWNT–PEI–Au/PB)_n$ modified electrode is synergetic result of factors demonstrated above. Finally, with the considerations of these findings, the $(MWNT–PEI–Au/PB)_n$ was chosen to be the final multilayer film for the immunosensor matrix.

In general, the sharp redox peaks of deposited PB layer can be attributed to the oxidation process as following equation (Mattos et al., 2000):

$$Fe^{III}_4[Fe^{II}(CN)_6]_3 + 4K^+ + 4e^- \leftrightarrow K_4Fe^{II}_4[Fe^{II}(CN)_6]_3 \quad (1)$$

The reduced form of Prussian white can be changed to be Prussian blue, accompanied with the loss of four electrons. Thus, the couple of well-defined peaks between −0.1 and 0.4 V were surely attributed to the conversion of Prussian blue and Prussian white. Any inhibitory event taken place on the surface of electrode will impede this conversion process by delaying electron transfer, thus, the peak current of electrode decreased. Based on this principle, the construction process for immunosensors can be characterized by CV. Fig. 3B shows the bare GC electrode had no CV response in the PBS (curve a in Fig. 3B). However, the GC/MWNT–PEI–Au had a greater background current response than the bare GC electrode (curve b in Fig. 3B), which suggests that the surface of the electrode was significantly covered by the MWNT–PEI–Au nanocomposite and electron transfer was improved (Ou et al., 2008; Cui et al., 2008). The GC electrode modified with $(MWNT–PEI–Au/PB)_5$ displayed well-defined peaks with the highest response (curve c in Fig. 3B). After the formation of the chitosan–Au film, the CV signal of GC/$(MWNT–PEI–Au/PB)_5$/(chitosan–Au) showed an obvious decrease (curve d in Fig. 3B). This behavior was the result of the inhibitory action of chitosan on the electron transfer of the electrode surface. Similarly, the CVs after coating with the antibody and blocking with BSA showed further inhibitory effects (curves e and f in Fig. 3B).

The relationship between the scan rate and CV peak current reflected the reaction kinetics change of the surface of electrode. The peak current linearly increased with the scan rate from 5 to 45 mV/s (see upper inset of Supplementary Fig. S2), which suggests that the observed electrochemical behavior was a surface process. However, the peak currents were proportional to the square root of the scan rate from 50 to 180 mV/s (see lower inset Supplementary Fig. S2), implied the current reaction kinetics changed from a surface process to a solution diffusion-confined process. The investigations above confirmed that the $(MWNT–PEI–Au/PB)_n$-modified electrode preserved the electrochemical activity of PB (Du et al., 2010).

3.3. Optimization

3.3.1. Optimization of fabrication process

To guarantee the good electrochemical behavior of the electrodes, some important parameters in the fabrication process and in the detection period need to be optimized. The CV results showed that the peak current reached a plateau when five cycles of electrodeposition on the surface of MWNT–PEI–Au were completed. Therefore, five cycles were chosen for fabrication throughout the experiments (see Supplementary Fig. S3).

The CV signal increased with an increasing number of bilayers. This phenomenon was attributed to the increased amount of Prussian blue loaded on the surface of the electrode. However, too thicker film may impede the electron transfer on the surface of the electrode (Bellezza et al., 2002). Thus, the number of (MWNT–PEI–Au/PB) bilayers should be considered carefully. The best response was reached when the number of bilayers was five (data not shown). Therefore, $(MWNT–PEI–Au/PB)_5$ was chosen for the final immunosensor matrix.

Synthesized gold nanoparticles can usually be used directly as the outermost layer by self-assembly or casting methods. Furthermore, the direct electrodeposition of gold nanoparticles onto the outermost surface of the electrode was also chosen because of its simplicity and ease of use, as already reported in several studies (Jiang et al., 2010; Ding et al., 2009; Yuan et al., 2007).

In this study, the chitosan–Au mixture was cast onto the surface of the modified electrode to fabricate a layer for immobilization of the antibody because chitosan had good biocompatibility and could effectively protect the inner matrix of electrode. However, the obvious immunoassay signal (ΔI) was not found for the immunosensor built from original synthesized gold nanoparticles mixed with chitosan. This observation could be attributed to an insufficient concentration of Au nanoparticles for effective antibody immobilization on the surface of the electrode. Thus, the immunoassay behavior of electrodes modified with different chitosan–Au mixtures was also investigated. The original concentration and 2, 5, 10, and 20-fold-concentrated gold nanoparticles were mixed with 1% chitosan at the ratio of 1:1 (v/v). The electrode modified with the 10-fold-concentrated gold nanoparticles mixed with chitosan provided the best electrochemical response to 10.0 ng/mL CEA (see Supplementary Fig. S4). The possible causes were attributed to the concentrated gold nanoparticles mixed in the chitosan not only effectively immobilized antibody, but also decreased the blocking effect of the chitosan. Consequently, the chitosan–Au mixture with 10-fold-concentrated Au nanoparticles was chosen to form outer layer film.

3.3.2. Optimization of analytical conditions

The parameters in the detection period, including the pH of the supporting electrolyte, immunoassay temperature and incubation time, were all considered. The investigation of different pH values of the supporting electrolyte was performed in 0.025 M PBS containing 0.1 M KCl. The highest response was found at pH 6.0, and the response then decreased at pH values above 7.0. This phenomenon was attributed to the instability of Prussian blue under alkaline conditions.

Although 37 °C was better for immunoreaction, a high temperature may damage the multilayer structure of (MWNT–PEI–Au/PB), so the final practical operating temperature was chosen to be 25 °C (Ou et al., 2008). Finally, the incubation time was chosen based on the effective decrease of current after the immunoreaction. With the addition of CEA, the decrease in current increased within 25 min and then reached a plateau. Thus, the effective time for immunoreactions was chosen to be 25 min.

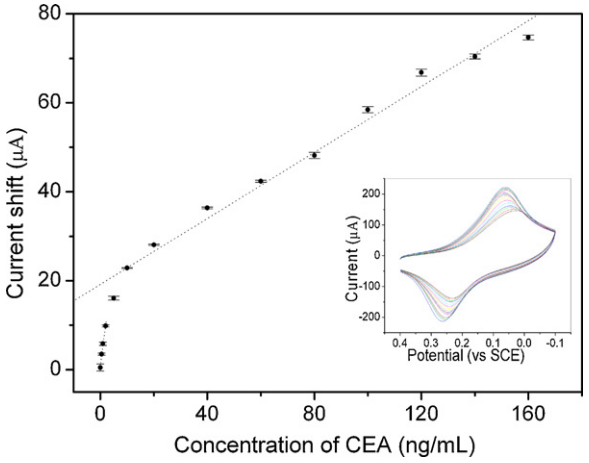

Fig. 4. The calibration curve of the reduction peak current response of the immunosensor (ΔI) vs. the concentration of CEA under optimal conditions. Inset: The CVs responses of the fabricated immunosensor to the different concentrations of CEA. The supporting electrolyte solution was 0.025 M PBS containing 0.1 M KCl, pH 6.0, scan rate of 50 mV/s vs. SCE.

3.4. The performance of the developed immunosensor for CEA

3.4.1. CV response and calibration curve

When the immunoassay reaction was taken place on the surface of electrode, the antigen–antibody complex will surely inhibited the electron-transfer. This action will lead to the change of the reduction current of immunosensor. With the successive addition of antigen, the proportional response to the different concentration of antigen can be observed. Under the optimized conditions, the amperometric response of the immunosensor to different concentrations of CEA antigen is shown in Fig. 4. The linear range of the $(MWNT–PEI–Au/PB)_5$/(chitosan–Au)/anti-CEA/BSA immunosensor was 0.5–2.0 ng/mL ($\Delta I = 4.58C_{CEA}$ (ng/mL) + 0.9, $r = 0.995$) and 2.0–160 ng/mL ($\Delta I = 0.37C_{CEA}$ (ng/mL) + 19.18, $r = 0.992$). The detection limit of the immunosensor was calculated to be 0.08 ng/mL (at 3δ). Furthermore, the presented immunosensor could easily respond to 0.5 ng/mL CEA antigen (inset of Fig. 4), which implied that the current immunosensor could achieve highly sensitive determination of low concentrations of CEA. This high sensitivity was mainly attributed to the effective immobilization of the anti-CEA by the chitosan–Au film and to the improvement of the conductivity between the electrode and PB by the MWNT–PEI–Au nanocomposite. The detection limit of present immunosensor is lower than the immunosensor based on PB (Lv et al., 2010). Besides, the linear range is wider than that of immunosensor based on Electrochemical impedance spectroscopy (EIS) (Tang et al., 2007), suggesting the present immunosensor will be apt to detect real sample.

3.4.2. Selectivity investigations

The selectivity of the immunosensor was carefully investigated. Some probable interfering compounds presented in the serum, including ascorbic acid, glycine, glucose, cysteine, BSA and Prostate specific antigen (PSA), were explored. The interference effect is evaluated by the current ratio (current ratio = I_1/I_2, I_1 was the current response of immunosensor in the CEA solution with interference and I_2 was the current response of immunosensor in the CEA solution without interference). The relative experimental results demonstrated the current ration ranged from 1.02 ± 0.02 to 1.05 ± 0.05 ($n = 5$), suggesting the present immunosensor was not significantly hindered by these interferences under physiological conditions.

Table 1
CEA concentration in blood samples tested by the immunosensor and ELISA method.

Serum sample	Immunosensor (ng/mL)[a]	ELISA (ng/mL)[a]	Relative deviation (%)
1	3.8 ± 0.1	3.6 ± 0.3	5.9
2	12.4 ± 0.5	12.8 ± 0.8	−3.1
3	27.4 ± 1.3	25.9 ± 0.9	5.8
4	49.1 ± 1.5	48.5 ± 0.8	1.2
5	67.3 ± 1.8	70.5 ± 1.6	−4.5

[a] Mean value ± SD of five measurements.

3.4.3. Reproducibility, regeneration and long-term stability

The reproducibility of the immunosensors was an important parameter for clinical application. In this study, the reproducibility of the immunosensor was investigated by analysis of the same samples (containing 20 ng/mL CEA) using five electrodes prepared in the same conditions. The reproductive measurements gave a relative standard deviation (RSD) of 4.9%. In addition, a RSD of 3.7% was obtained when the prepared immunosensor was carried out for five successive measurements of 20 ng/mL CEA.

The regeneration of the immunosensor was of interest for reducing the cost of real applications and for long-term reliability. Compared with the urea solution, the results of glycine-HCl buffer provided a better behavior of regenerated immunosensor. The RSD of renewed immunosensor regenerated by the later is 3.6%, and lower than that by urea solution. Moreover, as for the weak alkaline of urea solution, which may damage the fabricated PB layer, the glycine–HCl buffer was finally chosen as a reasonable solution for regeneration. The CV signal of the three immunosensors in the blank supporting electrolyte reached 94–97% of its initial response after the immunosensor was immersed in 0.1 M glycine–HCl solution (pH 3.5) for 15 min under stirring for the purpose of removing the antigen from Ab_1.

The final fabricated immunosensors were kept dry at 4 °C for 4 weeks, and the CV responses of the stored immunosensor retained 87.5% of their original value. These results suggest that the current electrode maintained its immunoactivity over long-term storage. The probable reasons were attributed to the following factors. First, the multilayer PB was stably anchored onto the surface of the MWNT–PEI–Au nanocomposite through strong electrostatic interactions. Second, the sandwiched multilayer structure based on this alternate strategy effectively maintained the stability of the nanocomposite film, and the layer of chitosan–Au played an important role in protecting the inner PB layer. Furthermore, the chitosan and gold nanoparticles had good biocompatibility and maintained the bioactivity of the antibody.

3.4.4. Application in real sample

The ability to determinate CEA in real serum is a key indicator for the potential application of the proposed immunosensor. To investigate the clinical potential of the current immunosensor, comparison experiments with enzyme-linked immunosorbent assay (ELISA) were performed by the detection of human serum. The results are shown in Table 1, suggesting the proposed immunosensor was feasible for the determination of CEA concentrations in clinical applications. Moreover, the recovery data were performed to assure this method (see Supplementary Table S1).

4. Conclusions

Through an alternate technique for electrodeposition and self-assembly, a novel immunosensor for the determination of CEA was developed. The ordered growing mode of the multilayer was confirmed by SEM and cyclic voltammetry. The present method effectively circumvented the drawbacks of one-step electrodeposition and illustrated the potential of this alternate strategy of electrodeposition and self-assembly in the construction of functional composite films. The resulting immunosensor demonstrated several advantages, including high sensitivity, a low detection limit and long-term stability. Furthermore, the construction process was simple, and the reproducibility of the electrodes was satisfactory. Thus, the present work demonstrates the potential application of the strategy of alternate electrodeposition and self-assembly in the development of novel immunosensors.

Acknowledgements

We acknowledge the Analytical Center of Zhejiang University providing access to TEM and Xia Li for help with TEM measurements. Furthermore, financial support from the National Natural Science Foundation of China (20805043, 30800247) is gratefully acknowledged.

Appendix A. Supplementary data

Supplementary data associated with this article can be found, in the online version, at doi:10.1016/j.bios.2012.02.063.

References

Bellezza, F., Cipiciani, A., Costantino, U., Negozio, M.E., 2002. Langmuir 18, 8737–8742.
Cioffi, M., Vietri, M.T., Gazzerro, P., Magnetta, R., D'Auria, A., Durante, A., Nola, E., Puca, G.A., Molinari, A.M., 2001. Lung Cancer 33, 163–169.
Clerico, A., Ry, S.D., Giannessi, D., 2000. Clin. Chem. 46, 1529–1534.
Chai, R., Yuan, R., Chai, Y.Q., Ou, C.F., Cao, S.R., Li, X.L., 2008. Talanta 74, 1330–1336.
Cui, R.J., Huang, H.P., Yin, Z.Z., Gao, D., Zhu, J.J., 2008. Biosens. Bioelectron. 23, 1666–1673.
Ding, C.F., Zhao, F., Ren, R., Lin, J.M., 2009. Talanta 78, 1148–1154.
Du, D., Wang, M.H., Qin, Y.H., Lin, Y.H., 2010. J. Mater. Chem. 20, 1532–1537.
Fiorito, P.A., Goncales, V.R., Ponzio, E.A., Torresi, S.I.C., 2005. Chem. Commun. 3, 366–368.
Gao, X., Zhang, Y.M., Chen, H., Chen, Z.C., Lin, X.F., 2011. Anal. Biochem. 414, 70–76.
Grabar, K.C., Freeman, R.G., Hommer, M.B., Natan, M.J., 1995. Anal. Chem. 67, 735–743.
Hage, D.S., 1999. Anal. Chem. 71, 294R–304R.
Haghighi, B., Varma, S., Alizadeh, F.M., Yigzaw, Y., Gorton, L., 2004. Talanta 64, 3–12.
Hornok, V., Dékány, I., 2007. J. Colloid Interface Sci. 309, 176–182.
Hu, X.G., Wang, T., Qu, X.H., Dong, S.J., 2006. J. Phys. Chem. B 110, 853–857.
Jiang, W., Yuan, R., Chai, Y.Q., Yin, B., 2010. Anal. Biochem. 407, 65–71.
Karyakin, A.A., Gitelmacher, O.V., Karyakina, E.E., 1995. Anal. Chem. 67, 2419–2423.
Liu, L.J., Zhang, F., Xi, F.N., Lin, X.F., 2008. Biosens. Bioelectron. 24, 306–312.
Liu, G.D., Lin, Y.H., 2006. Anal. Chem. 78, 835–843.
Li, Z.F., Chen, J.H., Li, W., Chen, K., Nie, L.H., Yao, S.Z., 2007. J. Electroanal. Chem. 603, 59–66.
Lukachova, L.V., Kotel'nikova, E.A., D'Ottavi, D., Shkerin, E.A., Karyakina, E.E., Moscone, D., Palleschi, G., Curulli, A., Karyakin, A.A., 2002. Bioelectrochemistry 55, 145–148.
Lv, P., Min, L.G., Yuan, R., Chai, Y.Q., Chen, S.H., 2010. Microchim. Acta 171, 297–304.
Matsumoto, K., Yuan, J.G., Wang, G.L., Kimura, H., 1999. Anal. Biochem. 276, 81–87.
Munge, B.S., Krause, C.E., Malhotra, R., Patel, V., Gutkind, J.S., Rusling, J.F., 2009. Electrochem. Commun. 11, 1009–1012.
Mattos, I.L., Gorton, L., Ruzgas, T., Karyakin, A.A., 2000. Anal. Sci. 16, 795–798.
Ou, C.F., Yuan, R., Chai, Y.Q., Tang, M.Y., Chai, R., He, X.L., 2007. Anal. Chim. Acta 603, 205–213.
Ou, C.F., Chen, S.H., Yuan, R., Chai, Y.Q., Zhong, X., 2008. J. Electroanal. Chem. 624, 287–292.
Qiu, J.D., Liang, R.P., Wang, R., Fan, L.X., Chen, Y.W., Xia, X.H., 2009. Biosens. Bioelectron. 25, 852–857.
Ricci, F., Palleschi, G., 2005. Biosens. Bioelectron. 21, 389–407.
Shi, W.T., Ma, Z.F., 2011. Biosens. Bioelectron. 26, 3068–3071.
Sharma, P., Sablok, K., Bhalla, V., Suri, C.R., 2011. Biosens. Bioelectron. 26, 4209–4212.
Song, Z.J., Yuan, R., Chai, Y.Q., Wang, J.F., Che, X., 2010. Sens. Actuators B: Chem. 145, 817–825.
Tang, H., Chen, J.H., Nie, L.H., Kuang, Y.F., Yao, S.Z., 2007. Biosens. Bioelectron. 22, 1061–1067.

Tlili, C., Cella, L.N., Myung, N.V., Shetty, V., Mulchandani, A., 2010. Analyst 135, 2637–2642.
Wu, J., Tang, J.H., Dai, Z., Yan, F., Ju, H.X., Murr, N.E., 2006. Biosens. Bioelectron. 22, 102–108.
Wu, Y., Zheng, J.W., Li, Z., Zhao, Y.R., Zhang, Y., 2009. Biosens. Bioelectron. 24, 1389–1393.
Worwood., M., 2002. Ann. Clin. Biochem. 39, 221–230.
Yuan, Y.R., Yuan, R., Chai, Y.Q., Zhuo, Y., Shi, Y.T., He, X.L., Miao, X.M., 2007. Electroanalysis 19, 1402–1410.
Zhuo., Y., Yuan, R., Chai, Y.Q., Tang, D.P., Zhang, Y., Wang, N., Li, X.L., Zhu, Q., 2005. Electrochem. Commun. 7, 355–360.
Zhang, Y.M., Gao, X., Chen, H., Chen, Z.C., Lin, X.F., 2012. J. Electrochem. Soc. 159, J17–J22.